Constrained Dewetting of Polymers Grafted onto a Nonadsorbing Surface in Poor Solvents: From Pancake Micelles to the Holey Layer

June Huh, Cheol-Hee Ahn, and Won Ho Jo*

Hyperstructured Organic Materials Research Center, and School of Materials Science and Engineering, Seoul National University, Seoul 151-742, Korea

Joanne N. Bright and David R. M. Williams*

Research School of Physical Science and Engineering, Australian National University, Canberra, ACT 0200, Australia

Received October 28, 2004; Revised Manuscript Received January 20, 2005

ABSTRACT: Using both theory and computer simulation, we study the dewetting problem of a polymer layer grafted on a surface in a poor solvent. We find that in the regime of moderate grafting density the layer is unstable to the formation of finite-sized holes. The formation of these holes is a result of the tradeoff between minimal layer surface energy and minimal tether penalty, thus giving an example of dewetting constrained by polymer stretching. We also examine the low-density case and find a new micellar regime where the nuclei of surface micelles are strongly flattened, forming "pancake micelles". The theoretical prediction qualitatively agrees with Monte Carlo simulations.

I. Introduction

The wetting and dewetting of liquid films on surfaces is one of the most fundamental and important properties of liquids. This phenomenon is of great practical importance in a number of industrial processes and attracts much interest from academia as well. The statics of wetting has been understood for a long time,[1] and there is now a partial understanding of the dynamics. The statics of wetting in its most basic form is very simple and is governed by three surface tensions which control the interfacial energies. A liquid will wet a surface if the total interfacial energy is lowered by doing so. This is the case for simple liquids such as water as well as for more complex liquids such as polymers.[2−6] It becomes complicated for very thin films where dispersion forces play a role; nevertheless, the statics in general is well understood. However, in one particular case, that of polymers end-tethered to a surface, the physics becomes much more subtle. In this case, we find a phenomenon which we call "constrained dewetting" or "constrained aggregation".

Systems of polymers end-tethered to a surface have extensively been studied over the past decade,[7,8] in part because they have been readily accessible experimentally and in part because they can apply to a variety of areas such as nanopatterning,[9] colloidal stabilization,[10] and block copolymer mesophases.[11] These systems are also of interest from a theoretical and fundamental point of view because they allow us to study chain deformation and cooperative effects. Much effort has focused on one corner of the phase diagram, i.e., the case of polymer in good solvent where the grafting density is so high that a uniform brush is produced.[7,8] Much less attention has been given to the case of poor solvents, where the monomer−monomer interaction is effectively attractive. In this case, however, a great deal of novel behavior has been predicted. In particular, in the regime of low grafting density, chains should form "octopus surface micelles" or "pinned micelles".[12−14] These are driven by a desire to avoid polymer−solvent contact and are opposed by a chain stretching penalty. They have been observed by both in computer simulations[15−17] and experiments.[18,19] In the high grafting density regime, another kind of instability has been predicted when the brush in a good solvent is gradually quenched into the poor solvent regime. In this case, the brush becomes unstable to formation of ripple.[20] The ripple arises because the chains stretch to form dense regions with favorable monomer−monomer contacts. However, as the solvent quality becomes poorer, the solvent molecules are expelled from the brush, removing the driving force for the instability, and as a result a melt brush is formed. This brush is stable against rippling, since rippling increases the surface energy.[21]

This is, however, not a complete picture of grafted polymers in poor solvents. In this paper, using both theory and computer simulation, we show new regimes where the previous prediction does not hold quantitatively or qualitatively. In particular, we show two major findings. First, at a moderate grafting density, a uniform layer is unstable to formation of holes that penetrate the entire layer. This forms a holey layer, with finite-sized holes, and is an example of dewetting constrained by polymer stretching. Second, the micellar regime discussed in previous work describes only a small part of the phase diagram, and there is a second micellar regime where the nuclei of surface micelles are strongly flattened, forming "pancake micelles".

Our attention in this paper is restricted to the case that polymer layers are grafted to nonadsorbing surface on which dewetting or polymer aggregation is constrained by polymer end-grafting. The case of polymers grafted to strongly adsorbing surface has been studied by Sevick and Williams.[23]

This paper is organized as follows. In the next section, the model and simulation method used for grafted polymer layers are briefly described. In section III, the simulation results are discussed and theoretically ana-

* Corresponding authors. E-mail whjpoly@plaza.snu.ac.kr (W.H.J.) or drw110@rsphysse.anu.edu.au (D.R.M.W.).

10.1021/ma047781z CCC: $30.25
Published on Web 02/24/2005

lyzed. Finally, we summarize our main findings in the last section.

II. Model and Simulation

A lattice-based dynamic Monte Carlo (MC) method is used to simulate the system of polymer chains that are grafted to a solid surface. Monodispersed polymer chains each consisting of N monomers are randomly grafted to impenetrable surface ($z = 0$) with grafting density ρ inside $96 \times 96 \times z$ cubic lattice ($z > N$), with periodic boundary condition in the x and y directions. Here, the grafting density ρ is defined as the number of grafted polymer chains per unit area. The monomer size and the lattice spacing are set to unity. The polymer chains are modeled to obey excluded-volume constraint, i.e., each lattice site can only be occupied by a monomer or be a void site, and all the void sites are regarded as solvents. The grafting density ranges from $\rho N = 0.1$ to $\rho N = 12$ with $N = 20-100$, which turns out to cover all the morphological regimes from micelle to uniform layer. Chain dynamics is implemented according to one-site bond fluctuation model (BFM) proposed by Shaffer[22] together with the Metropolis sampling scheme. This lattice chain dynamics have turned out to reproduce the dynamic properties of realistic chain molecule for short and long chain lengths.[22] The situation of poor solvent is modeled by applying an attractive interaction energy between two neighboring monomers ($\epsilon < 0$) while the monomer−solvent and the solvent−solvent interaction energies are put to be null. For the sake of simplicity, to model the situation of the nonadsorbing surface, it is assumed that the interaction between surface and monomer is the same as that between monomer and solvent; i.e., the surface tension forces solvent molecules to form a thin wetting layer between grafted layer and substrate. This makes the situation simpler and more symmetrical to model the polymer layer grafted on the nonadsorbing surface. We find that the introduction of different surface interaction does not alter qualitative or semiquantitative (scaling) behaviors of grafted layer unless the surface interaction with polymers is effectively attractive.

The initial configuration of a grafted polymer layer for a given set of ρ and N is prepared by simulating the system under athermal condition ($\epsilon/(k_BT) \equiv \epsilon' = 0$), which corresponds to the high-temperature limit. The temperature of system is then lowered from athermal state ($\epsilon/(k_BT) \equiv \epsilon' = 0$) to a target value of ϵ' by a stepwise temperature-lowering procedure with small lowering steps of $\Delta(N\epsilon') = 0.1$. At every temperature-lowering step reaching to a target value, the configuration obtained from the previous step is used as a starting point for a run at a lower temperature and then equilibrated for a time exceeding the relaxation time τ that is determined by measuring the decay of the autocorrelation function of a chosen observable (e.g., the height of grafted layer, the hole size in the case of holey layer). An example of the autocorrelation functions for the layer properties (the height of grafted layer h; the hole size R_h) is given in Figure 1. Furthermore, to check the equilibration of morphological formation particularly at high grafting densities, the system simulated at ϵ' is heated to $\epsilon' = 0$ and then cooled gradually back to ϵ' by the same temperature-lowering procedure used for the equilibration. We perform this sequentially to make ϵ' cycled up and down and monitor the morphological properties as a function of ϵ' cycles. Figure 2 demonstrates the morphological properties (the height of grafted layer h; the hole size R_h) of the grafted layer at a relatively high ρ as a function of the ϵ' cycles. No significant difference was found when the morphological properties between different cycles are compared to each other. Using this equilibration procedure, various layer properties such as the layer height are averaged over 50 independent runs.

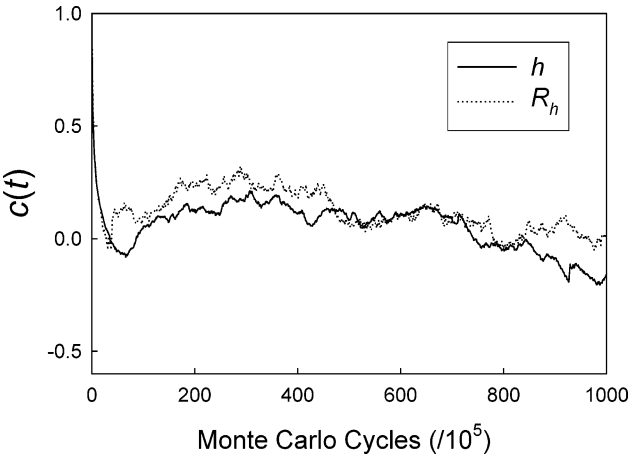

Figure 1. Autocorrelation functions $c(t)$ of layer properties as a function of Monte Carlo cycles for $N = 100$, $\epsilon' = -0.6$, and $\rho = 0.056$. The solid line represents the average height of the layer (R_h), and the dotted line represents the solvent-exposed surface area per a hole (h).

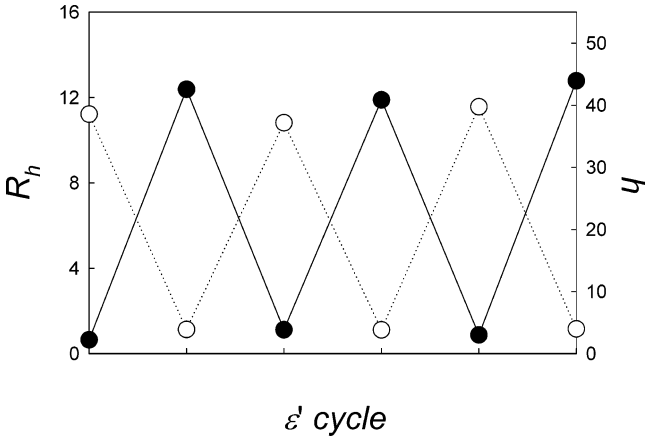

Figure 2. Properties of grafted polymer layer with $N = 100$ as a function of ϵ' cycles at $\rho = 0.056$. The filled circle represents the solvent-exposed surface area per a hole (R_h), and the open circle represents the average height of the layer (h).

III. Results and Discussion

Figure 3 shows the typical surface morphologies simulated at different grafting densities under a sufficiently poor solvent condition ($\epsilon' = -0.6$). As can be seen from the morphologies, in addition to classical structures, i.e., "octopus micelles" (Figures 3a and 2b) and "brush" (Figure 3d), an inverted form of micelles or a holey layer (Figure 3c) can be formed, which indicates that the previous picture for poorly solvated, grafted polymers covers only partial regions of grafting density. This is manifested by the scaling behavior of $h \sim \rho^{\nu}$ where h is the average height of the surface structure, as shown in Figure 4. The average height is calculated by $h = \int_0^\infty z\varphi(z)\,dz / \int_0^\infty \varphi(z)\,dz$, where $\varphi(z)$ is the monomer density profile in z. The plot shows that

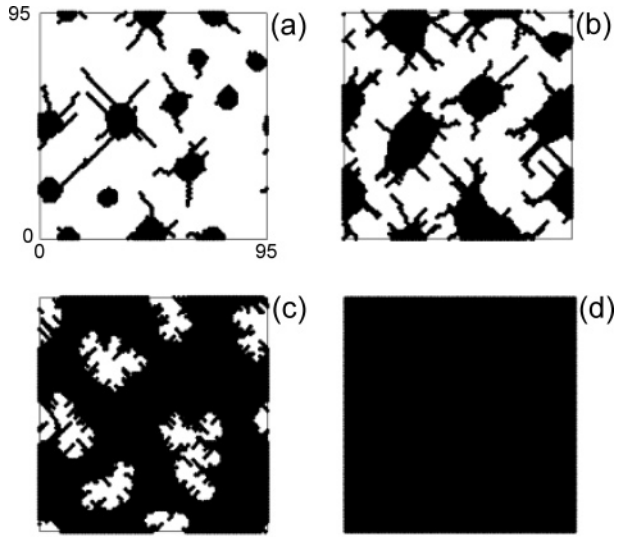

Figure 3. Two-dimensional snapshots of morphological structures simulated for $\epsilon' = -0.6$ and $N = 100$ at different grafting densities: (a) $\rho = 0.0067$, (b) $\rho = 0.025$, (c) $\rho = 0.056$, and (d) $\rho = 0.10$. The black regions represent polymer domains. The length scale is shown in units of the lattice spacing.

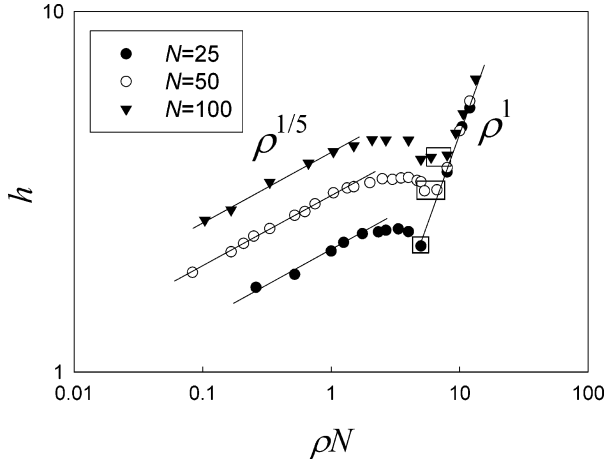

Figure 4. Average height of grafted layers as a function of the grafting density for $\epsilon' = -0.6$ at different values of N. The square boxes indicate the regions where the holey layer is observed.

at relatively low grafting densities $h \sim \rho^{1/5}$ for octopus micelles and very high grafting densities $h \sim \rho$ for brush, in agreement with the early scaling theories.[12−14] However, at the intermediate grafting densities where our study focuses on, the previously predicted scaling dependence does not hold any longer, and furthermore the height of surface structure is unexpectedly unchanged or even slightly decreases as the grafting density increases, indicating that the surface structure at those grafting densities becomes flat. These flat structures are micellar form or inverted micellar form (holey layer), as shown in Figure 3.

To theoretically examine the stability of these surface morphologies at intermediate grafting densities, we formulate the free energies of micelle and holey layer as follow. We begin with considering the case of holey layer. To do this, suppose circular holes of radius R_h "punched" in a layer. The pictorial representation of the geometry of a holey layer is given in Figure 5a. If the layer does not contain a hole (uniform layer), the free energy per unit area of the layer is given by the sum of a chain stretching term $\rho\pi^2 k_B T H_0^2/(24Na^2)$[24] and a

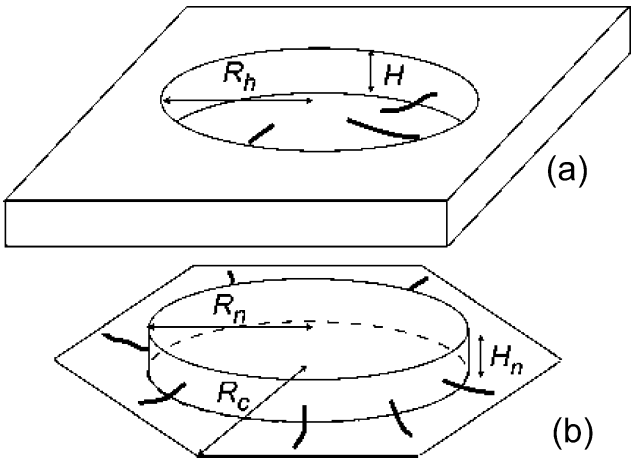

Figure 5. Pictorial representations of (a) a hole punched in a uniformly grafted polymer layer and (b) an octopus surface micelle.

surface energy 2γ (recall that the surface is covered with thin wetting layer of solvent), where a is the monomer size, γ is the polymer−solvent surface tension, and $H_0 = N\rho a^3$ is the height of the uniform layer. Formation of circular holes in the layer immediately reduces the surface energy by $2\pi\gamma R_h^2$, but at the same time, an extra lateral "rim" surface energy $2\pi\gamma R_h H$, a tether penalty for the chains that have grafting sites inside the hole, and extra layer stretching for the same chains when they enter the layer outside the hole, increases the free energy. To determine the size and stability of any possible hole, one needs to calculate the free energy including all these terms. The total free energy per unit area F_{HL} of a holey layer is expressed by the sum of three terms:

$$F_{HL} = F_{surf} + F_{tether} + F_{layer} \tag{1}$$

The surface free energy F_{surf} per unit area is given as

$$F_{surf} = 2\gamma(1 - m\pi R_h^2 + m\pi R_h H) \tag{2}$$

where m is the number of holes per unit area and H is the height of a holey layer. The layer height H is further expressed as follows. The chains which are grafted within the circular hole stretch radially outward, forming fully stretched tethers. This changes the layer height to

$$H = \frac{\rho Na^3 - \frac{2\pi\rho}{a}\int_0^{R_h}(Na - R_h + r)\,dr}{1 - m\pi R_h^2} = \frac{\rho a^2(3Na - m\pi R_h^3)}{3(1 - m\pi R_h^2)} \tag{3}$$

where r is the distance from the center of a hole. In calculating H, all chains grafted beneath the layer region contribute with their full volume Na^3, while those grafted in the hole region contribute only with those monomers not used for tether stretching, i.e., $(2\pi\rho/a)\int_0^{R_h}(Na - R_h + r)r\,dr$.

The contribution of tether F_{tether} consists of the surface energy and the stretching energy of tethers. Since each chain in the hole pays a penalty for stretching $k_B TD/(2a)$, where D is the distance stretched, and a surface

penalty $4\gamma Da$ (the chains have a square cross-section area a^2), the total contribution of tethers to the free energy per unit area is thus

$$F_{\text{tether}} = m\pi\rho\left(\frac{k_BT}{2a} + 4\gamma a\right)\int_0^{R_h}(R_h - r)r\,dr$$
$$= \frac{m\pi\rho R_h^3}{3}\left(\frac{k_BT}{2a} + 4\gamma a\right) \quad (4)$$

The third contribution F_{layer} in eq 1 accounts for the chain stretching within the layer. This can be calculated by assuming that all chains within the layer pay the same penalty. This means that although the tethers add different numbers of monomers to the layer, depending on the distance they have already stretched, there are chains of length Na stretching in the layer region with effective grafting density ρ_e:

$$\rho_e = \rho\left[1 - \frac{2m\pi}{Na}\int_0^{R_h}(R_h - r)r\,dr\right]$$
$$= \rho\left(1 - \frac{m\pi R_h^3}{3Na}\right) \quad (5)$$

The free energy of layer stretching per unit area can then be calculated from the layer energy given earlier, using an effective grafting density ρ_e and the layer height H:

$$F_{\text{layer}} = \frac{\rho_e\pi^2 k_BTH^2}{24Na^2} \quad (6)$$

From eqs 1−6, the final expression of total free energy per unit area is therefore

$$F_{\text{HL}} = 2\gamma\left[1 - m\pi R_h^2 + \frac{\pi R_h\rho ma^2(3Na - m\pi R_h^3)}{3(1 - m\pi R_h^2)}\right] + \frac{\pi\rho m(k_BT + 8\gamma a^2)R_h^3}{6a} + \frac{\pi^2 k_BT\rho^3 a(3Na - m\pi R_h^3)^3}{648N^2(1 - m\pi R_h^2)^2} \quad (7)$$

For a given ρ, N, and γ, the total free energy is minimized with respect to R_h and m. Typical results are shown in Figure 6 where the hole size R_h is plotted as a function of the surface tension, γ (theory), and as a function of ϵ' (simulation). What we find is that below a critical value, γ_c, the layer is stable against formation of holes. However, above γ_c a first-order transition takes place, and the layer can form holes. These holes have a finite size, and the system spontaneously dewets. Furthermore, it is found from eq 7 that above a critical value of ρ, $\rho_c = (\sqrt{6}/(4\sqrt{N}a^2))$, the system is unstable for no value of the surface tension; i.e., holes are never energetically favorable. For grafting densities close to this critical value, $\gamma_c = k_BTa^{-4}/(16(\rho_c - \rho))$. Note that at $\rho \approx a^{-2}N^{-1/2} \approx \rho_c$ the chains are roughly at their unperturbed length; i.e., the chains become stretched at ρ significantly higher than ρ_c. A typical value of γ_c can be found by setting $\rho = a^{-2}N^{-1/2}$. This gives $\gamma_c \sim k_BTa^{-2}$, which is a typical value for surface tensions in general. Thus, hole formation will occur in many experimentally accessible systems. This is an important result, showing an example of dewetting constrained by polymer stretching. From a practical point of view, grafted layers are often used as coatings. Our calculation shows that such layers may be unstable, particularly in very poor solvent such as air, and gives a criterion for stability against hole formation. Certainly, in most coating applications hole formation is disastrous.

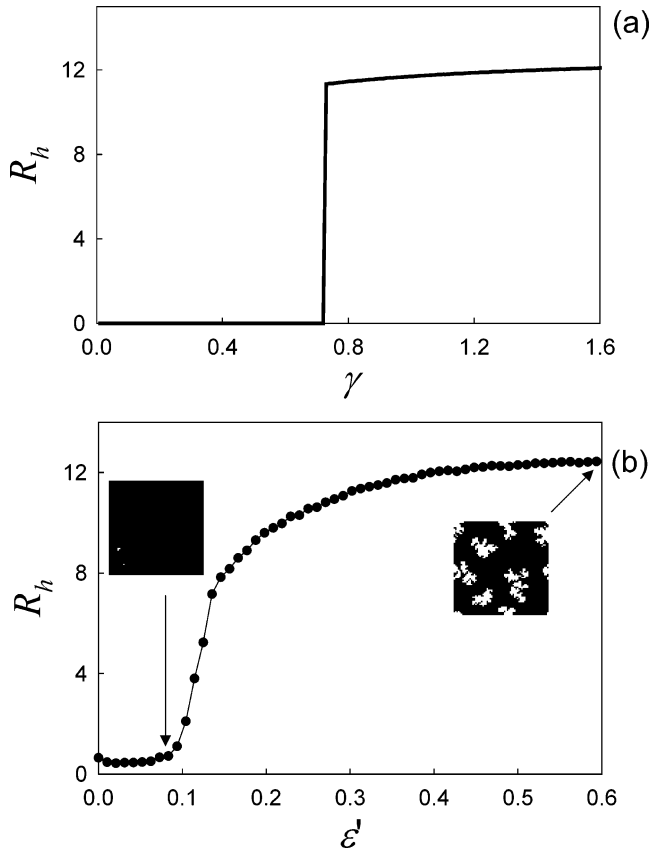

Figure 6. Theoretical prediction (a) and simulation result (b) of the hole size R_h as a function of γ (or ϵ') for a grafted layer with $N = 100$ and $\rho = 0.056$. In the theoretical result, k_BT and a are given to unity. In the simulation result, the hole size R_h is calculated from measurement of the exposed surface area $S = \pi R_h^2$.

We have just shown that a grafted layer is unstable to the formation of holes. However, it does not mean that a holey layer is the most stable state; it only means that it is more stable than a uniform layer. Furthermore, although the simulated morphology shows that a holey layer can be formed, it is also plausible that the simulated morphology shows only a kinetic intermediate. The true thermodynamic stability of holey layer should be therefore examined by comparing the free energy of holey layer with that of micellar morphology. Indeed, many of previous works on poor solvent systems have focused on a geometry, i.e., the spherical octopus micelle,[12−14] which is thought to be prevalent at low grafting densities. Each of these micelles consists of many chains stretched as tethers to form a large central globule or a "nucleus", i.e., a sphere with many legs stretching outward. The logic behind this geometry is simple. The chains want to minimize contact with solvent, and they can do this by fusing together to form a nucleus. The cost involved is that each chain must stretch toward the nucleus which involves a loss of entropy (chain stretching) as well as an exposure of the tethers to solvent. In the primitive theory, the balance of these effects gives the nucleus size of R_n ($=H/2$) $\propto N^{3/5}\rho^{1/5}$, and a grafting radius from which each micelle

takes its chains (the corona) $R_c \propto N^{2/5}\rho^{-1/5}$. Note that the number of micelles per unit area $p \propto R_c^{-2} \propto \rho^{2/5}$ increases with increasing the grafting density. The existence of these micelles and certain semiquantitative features has been supported by experiment and computer simulation. However, there were a number of approximations and simplifications in the early theories which we now question. The assumptions were (i) $R_n \ll R_c$, (ii) the nucleus is always spherical, (iii) the monomers used for forming a nucleus from the corona is neglected, (iv) the stretching within the nucleus is ignored, and (v) the packing of micellar corona is not taken into account. In this study, these assumptions are relaxed, and thus various micellar properties such as asphericity of micelle are examined. In principle, the nucleus could be of arbitrary shape. We model it as a cylinder of height H_n and radius R_n. This allow us to have a nucleus which has a form of roughly spherical, $H_n = R_n/2$, through pancake-shaped, $H_n \ll R_n$. We also consider the packing of micellar corona on the grafting surface. Previous studies assume a circular corona to minimize the free energy contribution from tethers that have to stretch toward the nucleus. However, there is certainly no way to tile whole grafting surface with such circles, and thus the contribution from the noncircular regions may not be negligible, particularly at high grafting densities. Here, we consider two cases of corona array: hexagonal and tetragonal packing. The pictorial representation of micelle geometry is given in Figure 5b.

We first consider the free energy of micelle in the hexagonal array. The free energy calculation is similar to the case of holey layer and includes terms describing the surface energy of the nucleus (F_{surf}), the stretching and surface penalties of the tethers (F_{tether}), and stretching within the nuclei (F_{nuclei}).

The total free energy per unit area for hexagonally arrayed micelles, F_{HM}, is

$$F_{HM} = F_{surf} + F_{tether} + F_{nuceli} \tag{8}$$

The surface energy per unit area is given by

$$F_{surf} = \frac{4\gamma\pi(R_n^2 + R_nH_n)}{3\sqrt{3}R_c^2} \tag{9}$$

where R_c is the distance from the micellar center to a vertex of the hexagon and H_n is the height of a nucleus H_n. Volume conservation for those monomers entering the nucleus yields the nucleus height:

$$H_n = \frac{\rho a^2(36\sqrt{3}aR_c^2N + 36\sqrt{3}R_c^2R_n - 3\sqrt{3}(4 + 3\ln 3)R_c^3 - 8\pi R_n^3)}{24\pi R_n^2} \tag{10}$$

The tether contribution F_{tether} is given as

$$F_{tether} = \frac{2X}{3\sqrt{3}R_c^2}\left(\frac{k_BT}{2a} + 4\gamma a\right) \tag{11}$$

where X is the total stretching distance for the tethers and is given by

$$X = \rho\left[\frac{\pi R_n^3}{3} + \left(\frac{\sqrt{3}}{2} + \frac{3\sqrt{3}}{8}\ln 3\right)R_c^3 - \frac{3\sqrt{3}}{2}R_c^2R_n\right] \tag{12}$$

The free energy of stretching within the nucleus per unit area is calculated using the nucleus height H_n and the effective grafting density $\rho_e = \rho - X/(Na)$:

$$F_{nuclei} = \frac{\pi^2\rho_eH_n^2}{36\sqrt{3}R_c^2Na^2} \tag{13}$$

The total free energy per unit area for hexagonally arrayed micelle is therefore

$$F_{HM} = \frac{2\gamma\rho a^2}{R_nR_c^2}\left[aR_c^2N + R_c^2R_n - \frac{2\sqrt{3}\pi}{27}R_n^3 - \frac{1}{12}R_c^3(4 + 3\ln 3)\right] + \frac{4\sqrt{3}\gamma\pi R_n^2}{9R_c^2} + \frac{\rho}{2aR_c^2}(8\gamma a^2 + k_BT)\left[\frac{2\sqrt{3}\pi}{27}R_n^3 + \frac{1}{12}R_c^3(4 + 3\ln 3) - R_c^2R_n\right] + \frac{9\rho^3ak_BT}{32N^2R_n^4R_c^2}\left[aR_c^2N + R_c^2R_n - \frac{2\sqrt{3}\pi}{27}R_n^3 - \frac{1}{12}R_c^3(4 + 3\ln 3)\right]^3 \tag{14}$$

The free energy for tetragonally arrayed micelles, F_{SM}, can be similarly formulated, and the final expression is

$$F_{SM} = \frac{\gamma\rho a^2}{18R_nR_c^2}[36aR_c^2N + 36R_c^2R_n - 3\pi R_n^3 - 12R_c^3(\sqrt{2} + \ln(1 + \sqrt{2}))] + \frac{\gamma\pi R_n^2}{2R_c^2} + \frac{\rho}{24aR_c^2}(8\gamma a^2 + k_BT)(\pi R_n^3 + 4R_c^3(\sqrt{2} + \ln(1 + \sqrt{2})) - 12R_c^2R_n) + \frac{\rho^3ak_BT}{2592N^2R_n^4R_c^2}(12a^2R_c^2N + 12R_c^2R_n - \pi R_n^3 - 4R_c^3(\sqrt{2} + \ln(1 + \sqrt{2})))^3 \tag{15}$$

The free energy of micelle for each case of micellar arrangement is then numerically minimized with respect to R_n and R_c.

By comparing four free energies (uniform layer, holey layer, and two cases of micelles) with each other, we can find which one is stable for a given ρ, N, and γ. Typical results of the free energies are plotted as a function of ρ, as shown in Figure 7. The free energy curves shows that micelles are stable at relatively low grafting density, whereas the holey layer is stable at a moderate grafting density between regime of micelle and uniform layer, although the region of stable holey layer is very narrow, and the free energy difference between micelle and holey layer is very small. However, we may expect that in a practical situation the holey layer can be found at a region of grafting density wider than that of theoretical prediction since the formation of micelles at high grafting densities might be kinetically hindered, and furthermore hole formation is a necessary intermediate stage in formation of micelles. It is also noteworthy that the free energy difference between two micelles with different packing of corona becomes larger as the grafting density increases. The simulated morphologies also show that the micellar arrangement becomes similar to hexagonal array as the grafting density increases (Figure 3a,b).

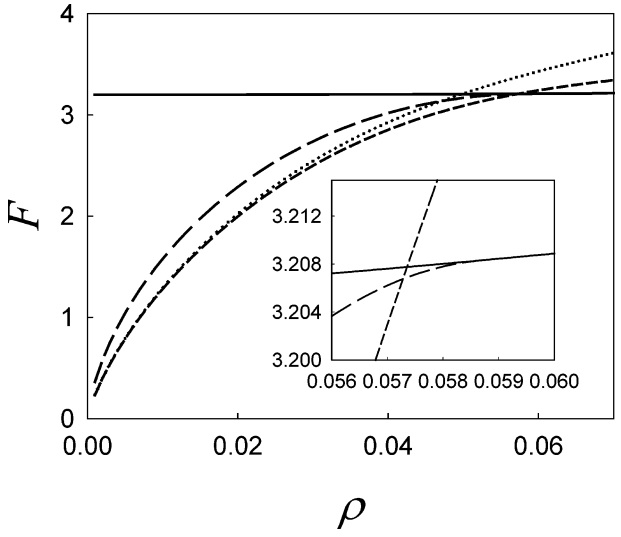

Figure 7. Free energies (F) of uniform layer (solid line), holey layer (long dashed line), micelles with hexagonally arrayed corona (short dashed line), and micelles with tetragonally arrayed corona (dotted line) as a function of grafting density. The parameters used are $N = 100$ and $\gamma = 1.6$. The inset shows the free energy curves with an enlarged scale at the intermediate grafting density where the holey layer is stable.

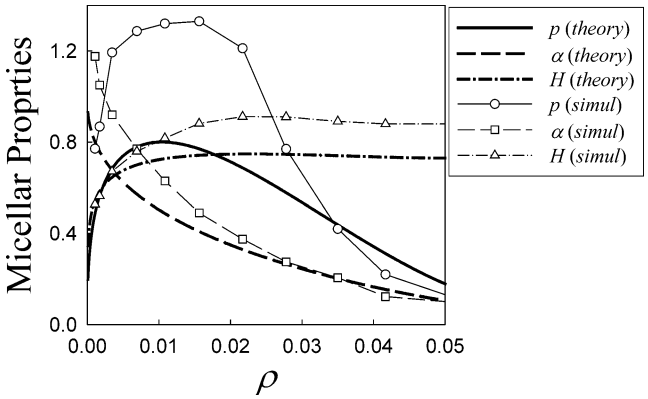

Figure 8. Plots of micellar properties against grafting density: the number of micelles per unit area, p (solid line, scaled by 1000); the aspect ratio α (dashed line, scaled by 0.5); and the height of nuclei H (dash−dotted line, scaled by 0.1). The parameters used are $N = 100$, $a = 1$, $k_BT = 1$, and $\gamma = 1.6$.

The micellar property at high grafting density differs from that predicted by the earlier studies in many respects. Figure 8 presents various micellar properties as a function of grafting density. Unexpectedly, it is found that the number of micelles per unit area $\pi = {}^2/_3\sqrt{3}R_c^2$ exhibits a maximum. The simulation result also confirms this maximum behavior despite some quantitative difference. At low grafting densities we recover the results predicted previously, i.e., $p \propto N^{-6/5}\rho^{2/5}$.[12−14] The maximum, however, was not previously predicted, and following the maximum there is a whole new micellar regime, where the number of micelles per unit area decreases as the grafting density increases. Previous work was based on the assumption that $R_n \ll R_c$; i.e., the nucleus is always much smaller than the corona. However, we find that the micellar behavior is more accurately described by $R_n \sim R_c$, with the corona rapidly disappearing at high grafting densities. Our results also indicate that the number of chains per micelle ($n \propto \rho R_c^2$) increases much more rapidly than the earlier theory suggests, implying that chains are "swallowed up" by the swelling nucleus as the grafting density increases. It is interesting to see the distortion of the micellar shape as this takes place. Figure 8 shows that the aspect ratio $\alpha \equiv H_n/R_n$ decreases monotonically and that $\alpha \approx 1$ at the maximum in p. The new scaling behavior is thus established when the micelle begins to deform from a sphere ($\alpha \approx 2$) to a pancake ($\alpha \to 0$). In this new regime, the micelle quickly flattens out until different micelles merge into each other, and as a result the system effectively creates holes. It should be stressed that the new micellar behaviors in the present model are mainly attributed to the release of the assumption for tethers that $R_n \ll R_c$ used in the previous study. Obviously, the tether penalty can be saved by decreasing the difference of $R_c - R_n$. At low grafting densities where the mean distance between grafting sites ($\sim\rho^{-2}$) is large, the assumption that $R_n \ll R_c$ is reasonable, and increasing grafting density creates more micelles; i.e., R_c decreases as ρ increases, since micelles are still too far from each other to fuse into larger micelles. In high grafting densities, however, the tether penalty can be largely saved by a rapidly swelling nucleus, i.e., R_n increases, rather than by decreasing R_c, and increasing grafting density results in fusion between different micelles. This further means that the number of chains per micelles increases more rapidly than the earlier model particulary at high grafting densities. These effects to save tether penalty at low and high grafting densities lead to the maximum behavior in p. Allowing asphericity of nucleus in the present model also has some effects on the maximum behavior since the formation of pancakelike micelle is certainly more advantageous to reduce the tether penalty $R_c - R_n$.

We have just shown that the layer with circular holes is stable at moderate grafting density between regime of micelle and uniform layer. However, the circular shape of hole is not the most favorable for our system for the following reason. If an ordinary liquid dewets the surface and forms a hole of fixed area πR_0^2 in the liquid, the shape of this hole would be a circle, since a circle minimizes the lateral surface area $2\pi R_0 H$, where H is thickness of the liquid film. In our system, it is not just the lateral surface area that must be minimized, but the combination of the lateral surface area and the tether penalty. The surface term favors a circular hole, but the tether term favors making all the tethers as close to the boundary as possible. More formally, for a given area we need to minimize $f = P + \Omega \int dx\, dy\, d_{min}(x, y)$, where P is the perimeter of the bounding curve, $d_{min}(x,y)$ is the distance from a point (x, y) inside the curve to a point on the curve, and the integral is taken over the area. Here $\Omega \equiv \rho(k_BT/a + 4\gamma a)/(\gamma H)$ measures how important the tethers are. We can examine the effect of a sinusoidal perturbation to the circular shape. Using the polar coordinates such a curve is expressed as $r(\theta) = R_0(\epsilon \cos(n\theta) + {}^1/_2\sqrt{4-2\epsilon^2})$ (see an example in Figure 9). To the second order in ϵ, we find $f = 2\pi R_0 + \pi R_0^3\Omega/3 + \pi(n^2 - 1)(R_0/2 - R_0^3\Omega/4)\epsilon^2$. From this it is clear that for $\Omega < \Omega_c$ ($= 2/R_0^2$) the circle is stable, but for $\Omega > \Omega_c$ the circular shape is unstable to crinkling. The simulated morphology of holey layer shown in Figure 3c also indicates that the boundary of hole is crinkling. This crinkling allows the tethers to reach the boundary more rapidly and hence lowers the free energy.

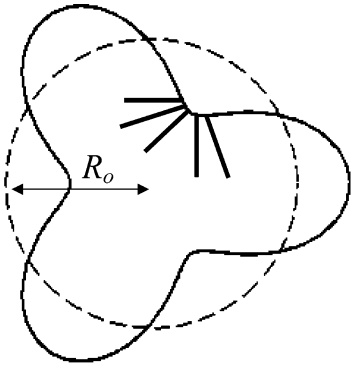

Figure 9. An example of crinkling hole expressed by $r(\theta) = R_0(\epsilon \cos(n\theta) + {}^1/_2\sqrt{4-2\epsilon^2})$ with $n = 3$ and $\epsilon = 0.5$. Note that the crinkling allows the tethers to reach the boundary more rapidly than the circular boundary.

IV. Summary and Concluding Remarks

In this paper, we have studied the dewetting problem of a polymer layer grafted on a surface in a poor solvent, focusing on the morphological formation of the grafted polymer layer at the intermediate grafting density. Both theoretical and MC simulation results show that the grafted polymers in poor solvent form pancakelike micelles or holey layer at the grafting density near the regime of uniform layer, which is result of the tradeoff between minimal layer surface energy and minimal tether penalty. These surface morphologies are qualitatively or quantitatively very different from that reported previously. We have also tried other geometries (square holes, overlapping spheres, stripes, toroids) to model the surface morphology at intermediate grafting density. None of these geometries proved more favorable than the geometries discussed above (pancake micelle, holey layer). Our theory and simulation model have several limitations. For instance, the use of surface tension γ to estimate the free energy cost of the tether is certainly a very crude approximation. Also, the use of the lattice geometry in the simulation has some effect on the morphological formation of grafted layer. Previously, Lai and Binder in their simulation work based on eight-site BFM reported that the monomer density profile of grafted layer in the z-direction becomes oscillatory at very low temperature, and such a tendency toward formation of crystal-like clusters may be largely due to the lattice artifact.[15] In our simulation based on one-site BFM, such oscillatory density profile is not observed up to $\epsilon' = -0.6$, which is the lowest temperature simulated in this study (Figure 10). Therefore, it is likely that one-site version of BFM dynamics mitigate such problem since one-site BFM has less dynamical constraints than eight-site BFM. According to our theoretical prediction and simulation, the holey layer is formed only at a narrow range of grafting densities, and therefore its stability seems still delicate matter. Nevertheless, we expect that in a practical situation the holey layer can be found at a region of grafting density wider than that of theoretical prediction since the formation of micelles with extremely flattened nuclei at high grafting densities might be kinetically hindered,

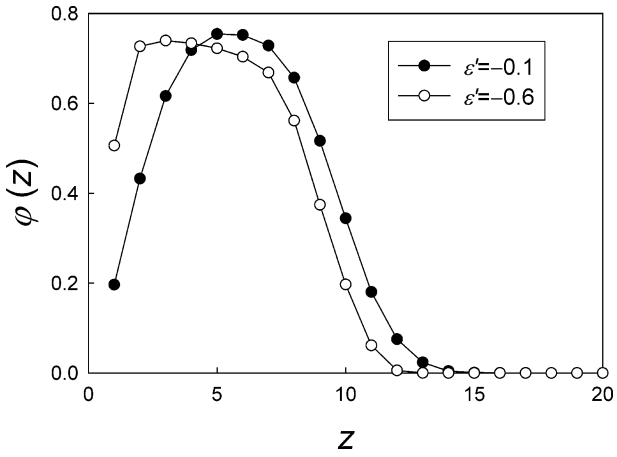

Figure 10. Monomer density profiles $\varphi(z)$ at $\epsilon' = -0.1$ and $\epsilon' = -0.6$ for $N = 100$ and $\rho = 0.056$.

and furthermore hole formation is a necessary intermediate stage in formation of micelles.

Acknowledgment. Financial support was provided by the Basic Research Program of Korea Science and Engineering Foundation (KOSEF) through Grant R08-2003-000-10461-0 and grants from the Australian Research Council. We thank Professor Anna C. Balazs at University of Pittsburgh for insightful discussions in the early stage of the work.

References and Notes

(1) de Gennes, P.-G. *Rev. Mod. Phys.* **1985**, *57*, 827.
(2) Brochard-Wyart, F.; de Gennes, P.-G.; Hervert, H.; Redon, C. *Langmuir* **1994**, *10*, 1566.
(3) Fondecave, R. F.; Brochard-Wyart, F. *Europhys. Lett.* **1997**, *37*, 115.
(4) Shull, K. R. *Macromolecules* **1996**, *29*, 8487.
(5) Reiter, G.; Auroy, P.; Auvray, L. *Macromolecules* **1996**, *29*, 2150.
(6) Sharma, A.; Reiter, G. *J. Colloid Interface Sci.* **1996**, *178*, 383.
(7) Halperin, A.; Tirrell, M.; Lodge, T. *Adv. Polym. Sci.* **1992**, *100*, 33.
(8) Milner, S. T. *Science* **1991**, *251*, 905.
(9) Minko, S.; Müller, M.; Usov, D.; Scholl, A.; Froeck, C.; Stamm, M. *Phys. Rev. Lett.* **2002**, *88*, 035502.
(10) Napper, D. M. *Polymeric Stabilization of Colloidal Dispersions*; Academic: New York, 1983.
(11) Fredrickson, G. H. *Macromolecules* **1993**, *26*, 4351.
(12) Williams, D. R. M. *J. Phys. II* **1993**, *3*, 1313.
(13) Zhulina, E. B.; Birshtein, T. M.; Priamitsyn, V. A.; Klushin, L. I. *Macromolecules* **1995**, *28*, 8612.
(14) Tang, H.; Szleifer, I. *Europhys. Lett.* **1994**, *28*, 19.
(15) Lai, P.-Y.; Binder, K. *J. Chem. Phys.* **1992**, *91*, 586.
(16) Soga, K. G.; Guo, H.; Zuckerman, H. J. *Europhys. Lett.* **1995**, *29*, 531.
(17) Grest, G. S.; Murat, M. *Macromolecules* **1993**, *26*, 3108.
(18) Stamouli, A.; Pelletier, E.; Koutsos, V.; vander Vegte, E. W.; Hadziioanou, G. *Langmuir* **1996**, *12*, 3221.
(19) Koutsos, V.; vander Vegte, E. W.; Pelletier, E.; Stamouli, A.; Hadziioanou, G. *Macromolecules* **1997**, *30*, 4719.
(20) Yeung, C.; Balazs, A. C.; Jasnow, D. *Macromolecules* **1993**, *26*, 1914.
(21) Solis, F. J.; Pickett, G. T. *Macromolecules* **1995**, *28*, 4307.
(22) Shaffer, J. S. *J. Chem. Phys.* **1994**, *101*, 4205.
(23) Sevick, E. M.; Williams, D. R. M. *Phys. Rev. Lett.* **1999**, *82*, 2701.
(24) Semenov, A. N. *Sov. Phys. JETP* **1985**, *61*, 733.

MA047781Z